

Two-dimensional Dirac nodal loop magnons in collinear antiferromagnets

S. A. Owerre¹

¹*Perimeter Institute for Theoretical Physics, 31 Caroline St. N., Waterloo, Ontario N2L 2Y5, Canada.*
(Dated: May 23, 2018)

We study the nontrivial linear magnon band crossings in the collinear antiferromagnets on the two-dimensional (2D) CaVO lattice, also realized in some iron-based superconductors such as $\text{AFe}_{1.6+x}\text{Se}_2$ ($A = \text{K, Rb, Cs}$). It is shown that the combination of space-inversion and time-reversal symmetry (\mathcal{PT} -symmetry) leads to doubly-degenerate eight magnon branches, which cross each other linearly along a one-dimensional loop in the 2D Brillouin zone. We show that the Dirac nodal loops (DNLs) are not present in the collinear ferromagnet on this lattice. Thus, the current 2D antiferromagnetic DNLs are symmetry-protected and they provide a novel platform to search for their analogs in 2D electronic antiferromagnetic systems.

The study of three-dimensional (3D) topological semimetals in electronic systems such as Dirac [1–5], Weyl [6–8], and nodal-line [9–14] semimetals has garnered considerable interest in condensed-matter physics. The Dirac and Weyl semimetals feature linear band crossing points at isolated points in momentum space that are topologically protected. Whereas the nodal-line semimetals feature symmetry-protected linear band crossing points along a one-dimensional (1D) loop in the 3D Brillouin zone (BZ). Indeed, the ubiquitous notion of topological semimetals is not restricted to electronic systems, and can also be applied to the band structures in bosonic systems. One of the areas currently attracting considerable attention is the topological linear magnon band crossing points in insulating magnetically ordered systems [15–17].

The topological linear magnon band crossing points occur at nonzero energy as a result of the bosonic nature of magnons. In this respect, realistic topological magnon semimetals with potential practical applications should involve the acoustic (lowest) magnon branch due to the population effect. By neglecting the Dzyaloshinskii-Moriya (DM) interaction [18, 19] in insulating quantum magnets, DNLs can exist in certain collinear ferromagnets [20–22]. Quite distinctively, 3D collinear [23] and noncollinear [17] antiferromagnets also allow 3D DNLs even in the presence of the DM interaction. In fact, 3D DNLs are theoretically prevalent in various 3D (layered) compounds when macroscopically symmetry-breaking terms are neglected.

Unlike 3D systems, the 2D analogs of DNLs are elusive and much less studied. They do not occur in simple 2D compounds. Recently, a handful of theoretical studies have proposed 2D DNLs in non-magnetic electronic systems with composite lattice structures such as honeycomb-kagomé lattice [24], mixed square lattice [25], and 2D trilayers [26]. However, the magnetic analogs of 2D DNLs are still elusive although various 2D magnetically ordered systems exist. Moreover, 2D antiferromagnetic (AFM) systems possess some unique features that make them theoretically and experimentally interesting. For instance, AFM systems form the basis of superconductors, and they are currently attracting much

attention in the field of spintronics [27, 28]. Therefore, the realization of 2D AFM DNLs may play a crucial role in condensed-matter physics. For collinear AFM systems, \mathcal{PT} -symmetry guarantees doubly-degenerate bands, therefore 2D AFM DNLs is not possible in simple ideal 2D honeycomb- and square-lattice antiferromagnets due to small unit cells.

In the current work, we circumvent these elusiveness by putting forward a new proposal for 2D AFM DNLs in collinear antiferromagnets on the CaVO lattice [29], named after the CaV_4O_9 compound [30, 31], which has a topologically equivalent lattice structure. Such lattice structure is also realized in iron-based superconductors such as $\text{AFe}_{1.6+x}\text{Se}_2$ ($A = \text{K, Rb, Cs}$) [32, 33]. The structure of this lattice is equivalent to a decorated (deformed) square lattice with two topologically inequivalent AFM nearest-neighbour bonds. The collinear antiferromagnet state on this lattice features eight sites in the unit cell. We show that the eight magnon branches are doubly-degenerate due to \mathcal{PT} -symmetry. Interestingly, they feature linear magnon band crossings along a 1D loop in the 2D BZ. We show that the loops of Dirac nodes are not present in the collinear ferromagnet on this lattice. Therefore, the 2D AFM DNLs are symmetry-protected and provide the first concrete example in 2D AFM systems.

We study the Heisenberg antiferromagnets on the CaVO lattice

$$\mathcal{H} = J \sum_{\langle ij \rangle} \vec{S}_i \cdot \vec{S}_j + J' \sum_{\langle ij \rangle'} \vec{S}_i \cdot \vec{S}_j. \quad (1)$$

There are two topologically inequivalent AFM bonds, namely J and J' . The first summation $\langle ij \rangle$ is taken over nearest-neighbour sites on the intralayer four-spin plaquettes, and the second summation $\langle ij \rangle'$ is taken over nearest-neighbour sites on the interlayer dimer bonds as depicted in Fig. 1a. We note that there is no geometrical spin frustration on this lattice for a wide range of J'/J [34]. Thus, the spins form a perfect collinear AFM structure with \mathcal{PT} symmetry. The perfect collinear AFM structure is accompanied by the presence of an inversion center, therefore the existence of the DM interaction is forbidden on the CaVO lattice. There are four sites per

structural unit cell, but the AFM unit cell contains eight sites, *i.e.* doubled as shown in Fig. 1(a). The CaVO lattice is also bipartite, and thus can be divided into two sublattices A and B.

We now study the magnetic excitations above the classical Néel ground state. For this purpose, it is expedient to introduce the Holstein Primakoff bosons:

$$S_i^z = S - a_i^\dagger a_i, \quad S_i^+ = \sqrt{2S} a_i = (S_i^-)^\dagger, \quad (2)$$

for up pointing spins,

$$S_j^z = -S + b_j^\dagger b_j, \quad S_j^+ = \sqrt{2S} b_j^\dagger = (S_j^-)^\dagger, \quad (3)$$

for down pointing spins. Here a_i^\dagger (b_i) are the bosonic creation (annihilation) operators on sublattice A (B), and $S_j^\pm = S_j^x \pm iS_j^y$ denote the spin raising and lowering operators. The bosonic hopping model is given by

$$\mathcal{H}_{\text{sw}} = S \sum_{\langle ij \rangle} J_{ij} [(a_i a_j^\dagger + b_j b_i^\dagger) + (a_i^\dagger b_j^\dagger + \text{h.c.})], \quad (4)$$

where $J_{ij} = J, J'$. The Fourier transformed Hamiltonian into momentum space yields $\mathcal{H}_{\text{sw}} = \sum_{\vec{k}} \Psi_{\vec{k}}^\dagger \mathcal{H}(\vec{k}) \Psi_{\vec{k}}$, where

$$\mathcal{H}(\vec{k}) = \begin{pmatrix} \mathcal{H}_+(\vec{k}) & 0 \\ 0 & \mathcal{H}_-(\vec{k}) \end{pmatrix}. \quad (5)$$

The basis vector is given by $\Psi_{\vec{k}}^\dagger = (\psi_{\vec{k}}^\dagger, \psi_{-\vec{k}}^\dagger)$, with $\psi_{\vec{k}}^\dagger = (a_{\vec{k}1}^\dagger, a_{\vec{k}2}^\dagger, a_{\vec{k}3}^\dagger, a_{\vec{k}4}^\dagger, b_{-\vec{k}5}, b_{-\vec{k}6}, b_{-\vec{k}7}, b_{-\vec{k}8})$. We note that each block Hamiltonian is an 8×8 Hermitian matrix representing $S_z = +1$ and $S_z = -1$ spin sectors that satisfies $\mathcal{H}_-(\vec{k}) = \mathcal{H}_+^*(-\vec{k})$. Therefore, $\mathcal{H}(\vec{k})$ is invariant under \mathcal{PT} symmetry given by $\mathcal{PT} = \sigma_x \otimes \sigma_0 \mathcal{K}$, where \mathcal{K} is complex conjugation, and σ_x is a Pauli matrix with an identity σ_0 . The Hamiltonian for the $S_z = +1$ sector is given by

$$\mathcal{H}_+(\vec{k}) = \begin{pmatrix} \mathcal{A}(\vec{k}) & \mathcal{B}(\vec{k}) \\ \mathcal{B}^*(-\vec{k}) & \mathcal{A}(\vec{k})^\dagger \end{pmatrix}, \quad (6)$$

with $\mathcal{A}(\vec{k}) = S(2J + J')\mathbf{I}_{4 \times 4}$, and $\mathcal{B}(\vec{k})$ is succinctly given by

$$\mathcal{B}(\vec{k}) = S \begin{pmatrix} 0 & J & J' e^{ik_y} & J \\ J & 0 & J & J' e^{ik_x} \\ J' e^{-ik_y} & J & 0 & J \\ J & J' e^{-ik_x} & J & 0 \end{pmatrix}, \quad (7)$$

where $\mathbf{I}_{4 \times 4}$ is the identity 4×4 matrix. The spin wave Hamiltonian $\mathcal{H}(\vec{k})$ can be diagonalized by the Bogoliubov transformation, and there are eight doubly-degenerate magnon branches due to \mathcal{PT} symmetry.

We now study the magnon band structure of collinear antiferromagnet on the CaVO lattice. For the purpose of comparison, we will also show the magnon band structure of corresponding collinear ferromagnet. These are

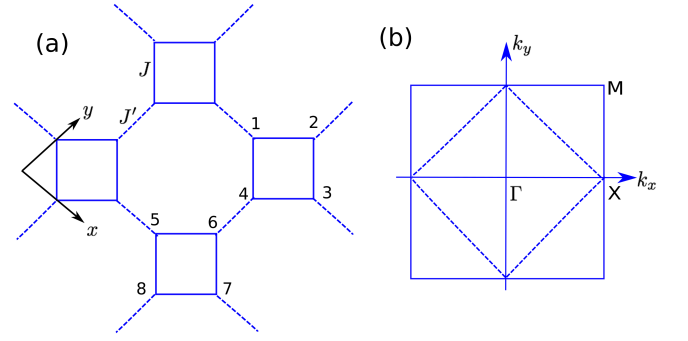


FIG. 1: (a) The CaVO lattice with two topologically inequivalent AFM bonds indicated by J and J' . The numbers label the 8-site AFM unit cell. (b) The corresponding square lattice BZ with high symmetry points indicated. The dashed square represents the AFM BZ.

shown in Figs. 2(a) and 2(b) respectively for $J'/J = 1$. In the collinear AFM case in Fig. 2(a), there are eight doubly-degenerate magnon branches. The magnon bands show linear Goldstone modes at the Γ and the M points of the BZ as expected in systems with a square lattice structure. Remarkably, the doubly-degenerate acoustic magnon band and the doubly-degenerate optical magnon bands feature a line of Dirac magnon nodes along the Γ - M line. The X point also contributes to the line of Dirac magnon nodes, with energy very close to those along the Γ - M line. Hence, the four-fold degenerate magnon band crossing forms a 1D curve as depicted in the inset of Fig. 2(a). Moreover, there also exists 2D magnon triple points (TPs) (six-fold degenerate) at the Γ and the M points. The TPs are isolated points and do not form line of Dirac magnon nodes.

For comparison, we have also shown the magnon band structures of the corresponding collinear ferromagnet in Fig. 2(b). In this case, there are only four sites in the unit cell and the four magnon branches are nondegenerate. In contrast to collinear antiferromagnets, there are no line of Dirac magnon nodes in the ferromagnetic system, however the TPs (three-fold degenerate in this case) are still present at the Γ and the M points, but at different energies. The existence of 2D TPs in both ferromagnets and antiferromagnets is due to \mathcal{C}_4 symmetry of the square lattice, and they are immediately gapped out for $J \neq J'$ [38] as shown in Figs. 2(c) and 2(d). In contrast, the 2D AFM line of Dirac magnon nodes are not a consequence of \mathcal{C}_4 symmetry and remain intact for $J \neq J'$, hence they are symmetry-protected by \mathcal{PT} symmetry of the collinear Néel structure.

Furthermore, the 2D linear magnon band crossings also form 1D loops in the 2D BZ plane centred at Γ , M and X points as shown in Figs. 3(a) and 3(b). It is noted that the TPs have no nodal-loop magnons in the 2D BZ as they are point nodes. Although the 2D AFM DNLs are symmetry-protected, we can further confirm their topological protection from the parity eigenvalues at the four time-reversal-invariant momenta in two dimensions

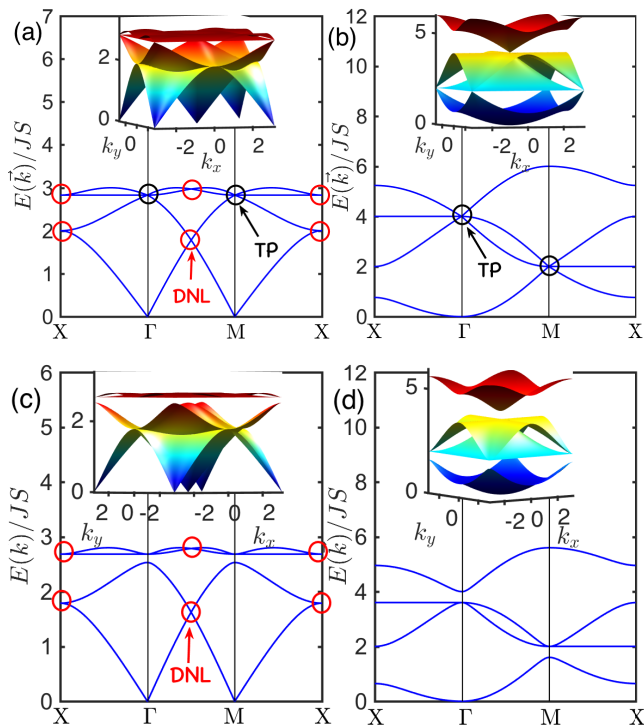


FIG. 2: (a,c) The doubly-degenerate eight magnon branches in the collinear antiferromagnet on the CaVO lattice for $J'/J = 1$ and $J'/J = 0.8$ respectively. (b,d) The non-degenerate four magnon branches in the collinear ferromagnet on the CaVO lattice for $J'/J = 1$ and $J'/J = 0.8$ respectively. The four-fold degenerate DNLs are indicated by the red circles, and the magnon triple points (TPs) (six-fold degenerate in the AFM phase and three-fold degenerate in the FM phase) are indicated by the black circles. Insets show the respective 3D magnon bands.

given by $\Gamma_i = \{(0, 0), (0, \pi), (\pi, 0), (\pi, \pi)\}$. The \mathbb{Z}_2 invariance ν is given by [36] $(-1)^\nu = \prod_{i=1}^4 \prod_{n=1}^N \xi_n(\Gamma_i)$, where $\xi_n(\Gamma_i)$ is the parity eigenvalue associated with the magnon bands that form DNLs. Numerical estimate shows that $\nu = 1$ which yields a nonzero topological invariant $\mathbb{Z}_2 = 1$, confirming the topological protection of the DNLs.

In a nutshell, we have shown that symmetry-protected 2D AFM DNLs exist in insulating collinear antiferromagnets on the CaVO lattice. The current 2D AFM DNLs occur at the acoustic magnon branch, which is very cru-

cial in realistic magnetic materials due to the population effect of bosons at low temperatures. Remarkably, the bosonic excitations could provide the realization of 2D AFM DNLs. They can be probed experimentally using the inelastic neutron scattering by synthesizing the right 2D AFM materials. The current results also provide a novel platform to search for 2D AFM DNLs in electronic systems. As we mentioned above, 2D AFM DNLs do not occur in the simple ideal 2D quantum antiferromagnets. For instance, the insulating collinear antiferromagnets on the square and honeycomb lattices have a single doubly-

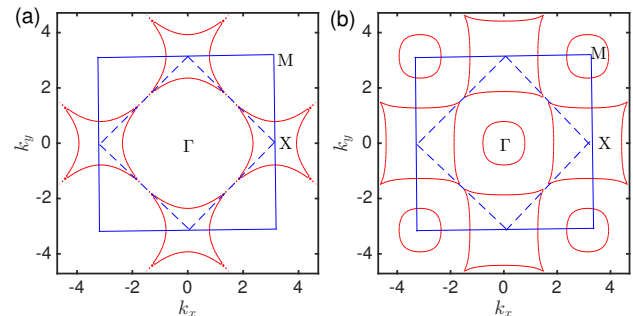


FIG. 3: Loops of Dirac magnon nodes formed by (a) the acoustic magnon band crossing and (b) the optical magnon band crossing. The solid rectangles denote the structural BZ with high symmetry points indicated, and the dashed squares represent the AFM BZ zone. We set $J'/J = 1$ corresponding to Fig. 2(a).

degenerate magnon branch, which cannot possess linear band crossing between two magnon branches in the BZ. The proper inclusion of the DM interaction should lead to spin canting and noncollinear spin structure. However, a small DM interaction will not completely eliminate the DNLs in the entire BZ due to the high symmetry protection of the lattice. Since there is no experimental evidence of the DM interaction on the current lattice, we believe that the DNLs should be present and robust. Upon the completion of this paper, we became aware of a recent arXiv preprint [37], where 2D DNLs have been proposed in an electronic AFM system, but with nonsymmorphic analogue symmetry as opposed to \mathcal{PT} symmetry.

Research at Perimeter Institute is supported by the Government of Canada through Industry Canada and by the Province of Ontario through the Ministry of Research and Innovation.

[1] S. M. Young et al. Phys. Rev. Lett. **108**, 140405 (2012).
 [2] Z. Wang et al. Phys. Rev. B **85**, 195320 (2012).
 [3] Z. K. Liu et al. Nat. Mater. **13**, 677 (2014).
 [4] S. -Y. Xu et al. Science **347**, 294 (2015).
 [5] P. Tang et al. Nat. Phys. **12**, 1100 (2016).
 [6] X. Wan et al. Phys. Rev. B **83**, 205101 (2011).
 [7] S. -Y. Xu et al., Science **349**, 613 (2015).

[8] B. Q. Lv et al. Phys. Rev. X **5**, 031013 (2015).
 [9] C. Fang et al. Phys. Rev. B **92**, 081201 (2015).
 [10] A. A. Burkov, M. D. Hook, and L. Balents, Phys. Rev. B **84**, 235126 (2011).
 [11] T. Bzdusek et al. Nature **538**, 75 (2016).
 [12] H. Huang et al. Phys. Rev. B. **93**, 201114(R) (2016).
 [13] G. Bian et al. Nat. Commun. **7**, 10556 (2016).

- [14] J. Wang, Phys. Rev. B **96**, 081107 (2017).
- [15] F. -Y. Li et al. Nat. Commun. **7**, 12691 (2016).
- [16] A. Mook, J. Henk, and I. Mertig, Phys. Rev. Lett. **117**, 157204 (2016).
- [17] S. A. Owerre, Phys. Rev. B **97**, 094412 (2018).
- [18] I. Dzyaloshinsky, J. Phys. Chem. Solids **4**, 241 (1958).
- [19] T. Moriya, Phys. Rev. **120**, 91 (1960).
- [20] A. Mook, J. Henk, and I. Mertig, Phys. Rev. B **95**, 014418 (2017).
- [21] S. A. Owerre, Sci. Rep. **7**, 6931 (2017).
- [22] S. S. Pershoguba et al., Phys. Rev. X, **8** 011010 (2018).
- [23] K. Li et al., Phys. Rev. Lett. **119**, 247202 (2017).
- [24] J. L. Lu et al. Chin. Phys. Lett. **34** 057302 (2017).
- [25] B. Yang, X. Zhang, and M. Zhao, Nanoscale, **9**, 8740 (2017).
- [26] C. Niu et al. Phys. Rev. B **95**, 235138 (2017).
- [27] T. Jungwirth et al. Nat. Nanotech. **11**, 231 (2016).
- [28] V. Baltz et al. Rev. Mod. Phys. **90**, 015005 (2018).
- [29] J. Richter, J. Schulenberg and A. Honecker in *Quantum magnetism in two dimensions: from semi-classical Neel order to magnetic disorder*. Lect. Notes Phys. **645**, 85 (2004). arXiv:cond-mat/0412662
- [30] S. Taniguchi et al. J. Phys. Soc. Jpn. **64**, 2758 (1995).
- [31] K. Ueda, H. Kontani, M. Sigrist and P. A. Lee, Phys. Rev. Lett. **76**, 1932 (1996).
- [32] M. Wang et al. Nat. Commun. **2**, 580 (2011).
- [33] P. Dai, Rev. Mod. Phys. **87**, 855 (2015).
- [34] L. O. Manuel, M. I. Micheletti, A. E. Trumper, H. A. Ceccatto, Phys. Rev. B **58**, 8490 (1998).
- [35] S. A. Owerre, Europhys. Lett. **120**, 57002 (2017).
- [36] L. Fu and C.L. Kane, Phys. Rev. B **76**, 045302 (2007).
- [37] B. Wang et al., arXiv:1803.04133 (2018).
- [38] Unlike 2D systems, 3D magnon TPs are robust against magnetic anisotropy as well as the DM interaction, see Ref. [35]